JOURNAL OF MATERIALS SCIENCE 31 (1996) 3623–3637

Densification of ultrafine SiC powders

R. VAßEN, A. KAISER, J. FÖRSTER, H. P. BUCHKREMER, D. STÖVER
Institut für Werkstoffe der Energietechnik, Forschungszentrum Jülich, 52425 Jülich, Germany

Recent results on the densification behaviour of ultrafine SiC powders (below 20 nm) are presented and compared with results on the densification of ultrafine silicon-based ceramic powders given in the literature. A study of different powder processing routes and their influence on the pore-size distribution is given. Pressureless sintered green bodies having pore sizes of about 20 nm show extreme coarsening without significant densification. The results indicate a significant influence of green density on shrinkage. Encapsulated hot isostatic pressing (HIPing) led to a reduction of pore size and to considerable density increase at temperatures below 1600 °C. But even then full density without extensive grain growth was difficult to achieve. The applied method to determine grain sizes (X-ray diffraction measurements, XRD, using the Scherrer formula, scanning electron microscopy, SEM, and transmission electron microscopy, TEM) gave similar results for TEM and SEM but lower values for XRD. A possible explanation is presented. Density and grain growth both during pressureless sintering and HIPing showed significant differences between samples with and without sintering additives (B and C). Whether or not the use of sintering agents is favourable in reaching high densities and fine grain sizes, is discussed. HIP densification was modelled assuming diffusion to be the dominant mechanism. Grain growth according to a $t^{1/4}$ dependence and an activation energy of 6.8 eV was introduced into the model. Results on the properties (hardness, also at elevated temperatures, fracture toughness, bending and compression tests, thermal conductivity) of the hot isostatically pressed samples, are presented.

1. Introduction

Silicon carbide is a promising candidate for high-temperature structural applications because of its combination of properties, such as excellent high-temperature strength and good oxidation, creep and thermal shock resistance [1–3]. Despite these properties, widespread use of (SiC) ceramics still requires a significant improvement in fracture toughness and reliability. As pointed out by several authors [4–6] a promising way to achieve this aim might be the reduction of grain size down to the nanosized range. Although an improvement of fracture toughness at room temperature due to plastic deformation seems to be unlikely in nanophase SiC [7], an improvement of strength and reliability is expected. This requires an optimized processing of the ultrafine starting powders (i.e. large agglomerates should be avoided or destroyed during processing routes and grain growth is minimized). The resultant densified material will then exhibit a defect size which is of the order of the grain size. Fracture strength, as well as reliability, will increase.

For oxide ceramics (doped zirconia [8] or titania [6]), it has been demonstrated that a dense, nanocrystalline (grain size below 100 nm) material can be produced by pressureless sintering if the pore to grain diameter ratio does not exceed a critical value [9]. Much work has also been performed on the densification of ultrafine covalently bound powders. Several authors have found that the sintering of ultrafine silicon powders to densities greater than 90% theoretical led to grain growth up to more than 200 nm [10, 11]. HIPing of ultrafine Si_3N_4 powders [12] resulted in grain sizes of about 500 nm and densities of 90% theoretical. As shown in the discussion of the present work, similar results can also be found in the literature for the densification of ultrafine SiC powders. This seems to indicate that the manufacture of nanophase covalently bound materials is difficult, even when pressure-assisted sintering is used.

In order to improve the unfavourable ratio between grain growth and densification, further information on the densification process would be useful. The main variables which determine the densification process or the sintering rate are mass transport (e.g. diffusion), driving forces such as surface curvature and HIP pressure, as well as grain size, grain growth, and the pore-size distribution of the green body. As shown in the present work, the influence of the green body microstructure can be reduced by applying pressure-assisted sintering. The enhancement of the neck growth rate in the final stage, by the HIP pressure is probably of lesser importance because the actual sintering pressure ($2\gamma/r \approx 500$ MPa with $\gamma = 1.85\ J\,m^{-2}$ [13]) is comparable to the pressures used in

0022–2461

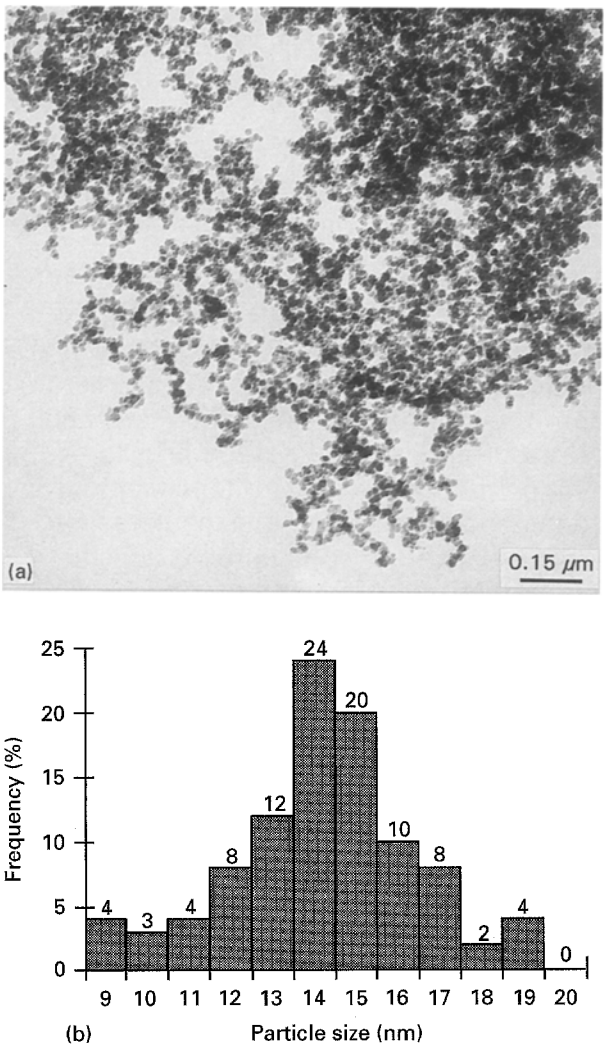

Figure 1 (a) Micrograph and (b) particle-size distribution of laser-synthesized SiC powders.

conventional HIPing (200 MPa). In the present investigation, this situation is improved by increasing the HIP pressure up to 350 MPa.

A deeper insight in the influence of process parameters such as temperature, HIP pressure, sinter time, and pore-size distribution of the green body, on the densification of ultrafine SiC powders, can be obtained if a theoretical description of the densification results is possible. Therefore, experimental results were compared with common models for grain growth and HIP densification.

2. Experimental procedure

2.1. Powder synthesis and characterization

Nanophase β-SiC powders (Fig. 1a) were produced at the Institut für Laser- und Plasmaphysik, Universität Düsseldorf, Germany, by a CO_2 laser-assisted synthesis using a mixture of SiH_4 and C_2H_4 as gas-phase precursors [14, 15]. The laser power was 100 W, the chamber pressure 50 kPa and the silane and acetylene flows 333 and 167 standard $cm^3\,min^{-1}$, respectively. In some cases, the sinter additive, boron, was introduced during the laser synthesis by adding diborane to the reactant gases. These powders are denoted SiCB. The powders can be produced at a production rate of about $50\,g\,h^{-1}$. After filling into a 10 l steel vessel (capacity $\approx$ 200 g) the powders are transported under an argon atmosphere to the KFA-Jülich and introduced into an argon filled glove box without contact with air. The subsequent processing steps were also performed under inert gas conditions.

The produced particles showed an extremely narrow particle-size distribution. The mean particle size measured using a transmission electron microscope (TEM) was 15 nm for the SiC and 13 for the SiCB powder. The extremely narrow particle-size distribution is given in Fig. 1. BET analysis gave surface areas of 104 and $126\,m^2\,g^{-1}$ for the ultrafine SiC and the SiCB powders, respectively. These values correspond to spherical particles with diameters of 17.8 and 14.8 nm in good agreement with the TEM results. X-ray diffraction measurements revealed partially amorphous structures with broad β–SiC peaks. A linewidth analysis (Scherrer formula [16]) resulted in crystallite sizes of 3–5 nm indicating that each powder particle consists of approximately 20–100 individual grains.

The results of a chemical analysis of the ultrafine powders approximately 1 week after production are given in Table I. In some cases, amorphous boron (HC Starck $\approx$ 830 nm) and/or carbon (Lonza, KS6, $\approx$ 500 nm) as sintering additives were added during the agglomeration step (see below). For comparison, SiC powder from HC Starck (B20, $\approx$ 500 nm) was also used.

2.1.1. Powder processing

Owing to the extremely low density of the as-prepared powders ($\approx$ 0.6% theoretical [17]), the powders were agglomerated by dispersing them in ethanol (with SiC balls) in a Turbula mixer for about 24 h and afterwards dried under reduced pressure and at elevated temperature (70 °C). The SiC powder subsequently showed an apparent density of 11% theoretical, which was sufficient for the succeeding cold isostatic pressing step (CIP). Green bodies produced by CIPing had cylindrical geometries with diameters between 7 and 12 mm and lengths between 40 and 60 mm; densities of 38%–42% theoretical were obtained. SiCB powders had a lower density of about 4.4% theoretical after the agglomeration step. Therefore, these powders were CIPed at 100 MPa and ground. The powder density was increased to about 13% theoretical, subsequent CIPing led to green densities of 31% theoretical. The significant lower powder density of ultrafine SiCB powders compared to SiC powders might be a result of the smaller particle size ([17]) and/or the surface modification due to the addition of boron.

In order to analyse the influence of solvent and drying process, water instead of ethanol was used. The mixtures were dried by freeze drying as well as by the conventional method. Furthermore, powders were also agglomerated by cold isostatic pressing (250 MPa) to avoid the drying process.

TABLE I Results of the chemical analysis of the laser-synthesized powders

Powder	Silicon (wt %)	Carbon (wt %)	Oxygen (wt %)	Boron (wt %)	Total (%)
SiC	66.20 ± 2.00	31.4 ± 0.35	1.01 ± 0.11	–	98.61
SiCB	64.74 ± 1.94	28.0 ± 0.8	1.49 ± 0.03	4.04 ± 0.12	98.27

2.1.2. Sintering

Pressureless sintering of the green bodies was performed under a vacuum in a graphite furnace.

2.1.3. Hot isostatic pressing

CIPed cylinders were filled into glass capsules with a BN or, in a few cases, a carbon (foil) interlayer. In the intermediate temperature (1500–1700 °C) range, borosilicate glasses produced by Schott or Corning (Vycor) were used. In HIP runs performed at lower temperatures, capsules were made of Duran glass, and at higher temperature quartz glass was used. Before HIPing, the capsules were degassed in a vacuum furnace ($< 10^{-3}$ mbar) at 400–800 °C and afterwards sealed under vacuum. HIPing was performed in two facilities produced by National Forge, Belgium, with pressures in the range between 100 and 350 MPa. The dwell time varied between 10 min and 4 h. Heating rates were 15 K min^{-1} up to 1350 °C. Afterwards pressure and temperature were increased at about 6 MPa min^{-1} up to the final pressure and temperature.

2.2. Analysis of microstructure and evaluation of mechanical properties

Densities of the composites were measured by Archimedes' method. For the theoretical density of SiC, 3.21 g cm^{-3} was taken.

Using X-ray diffraction, the constitution of the composites was determined and line broadening was used to calculate the grain size from the Scherrer formula. Chemical analysis was performed to determine the carbon content (LECO system), the oxygen and nitrogen content (hot gas extraction with thermal conductivity measurement and infrared spectroscopy, respectively), and the silicon and boron content (inductively coupled plasma–optical emission spectroscopy). Porosity distributions were determined in a micromeritics autopore mercury porosimeter.

Microstructure was investigated by scanning electron microscopy (SEM) mainly on fracture surfaces of the composites. The SEM was a Jeol JSM T300 operating at 25 keV. Grain sizes were estimated by multiplying the mean diameter determined from fracture surfaces by a factor of 1.2 [18]. TEM investigations were performed with a Philips transmission electron microscope (EM 430, 300 kV).

Mechanical properties, such as hardness and fracture toughness, were evaluated at room temperature. Hardness tests were performed with a Vickers hardness tester operating with a load of 10 kg and a loading time of 15 s. Fracture toughness, K_{Ic}, was measured by the indentation fracture method [19], using an optical microscope at a magnification of × 500. For one specimen, the hardness at 800, 1000, and 1100 °C was measured at the Lehr- und Forschungsgebiet Werkstoffkunde, University of Aachen [20]. Also a three-point bending test with fixed rods and 17 mm span was performed. Cylindrical specimens with a diameter of about 5 mm have been used in compression tests at 1400 °C.

Thermal conductivity was measured at room temperature by measuring the temperature gradient, which is established by heating one side of the cylindrical specimen with a known electrical power, and cooling the other side.

3. Results and discussion

3.1. Powder processing

Fig. 2 shows the results of pore-size measurements of cold isostatically pressed green bodies. The used powders were processed by the different methods given in Section 2. Table II gives further information on the samples. Chemical analysis was performed 36/68/82 days after powder production. While the carbon content remains approximately constant (only the dry processed powder revealed one extremely low value which cannot be explained), the oxygen content of the pressed and freeze dried powder increases with storage time. Although storage was performed under argon, it is difficult to avoid oxygen contact completely. The final amount of 1.9 wt % oxygen is equal to about half a monolayer of oxygen which is formed within hours if the powders are exposed to air [21]. Powders which are mixed in water and dried conventionally show this oxygen amount for all measurements. They probably pick up the oxygen during the drying step.

Table II and Fig. 2 reveal that the first three processing methods lead to only slightly different pore-size distributions within the green bodies. The large deviations in the apparent densities might partly be due to different pore volumes which cannot be filled by mercury. The higher total pore area of the CIPed freeze dried powder might be explained by the avoidance of a liquid/vapour interface during solvent removal. An evaporating liquid pulls the powder particles together due to capillary forces, leading to closer contacts between the particles, i.e. harder agglomerates with a reduced free surface. On the other hand, one would also expect an increase in the average pore diameter and a decrease in green density in the case of freeze dried powder, which is not observed.

Processing with ethanol leads to larger pore diameters and higher green densities compared to the

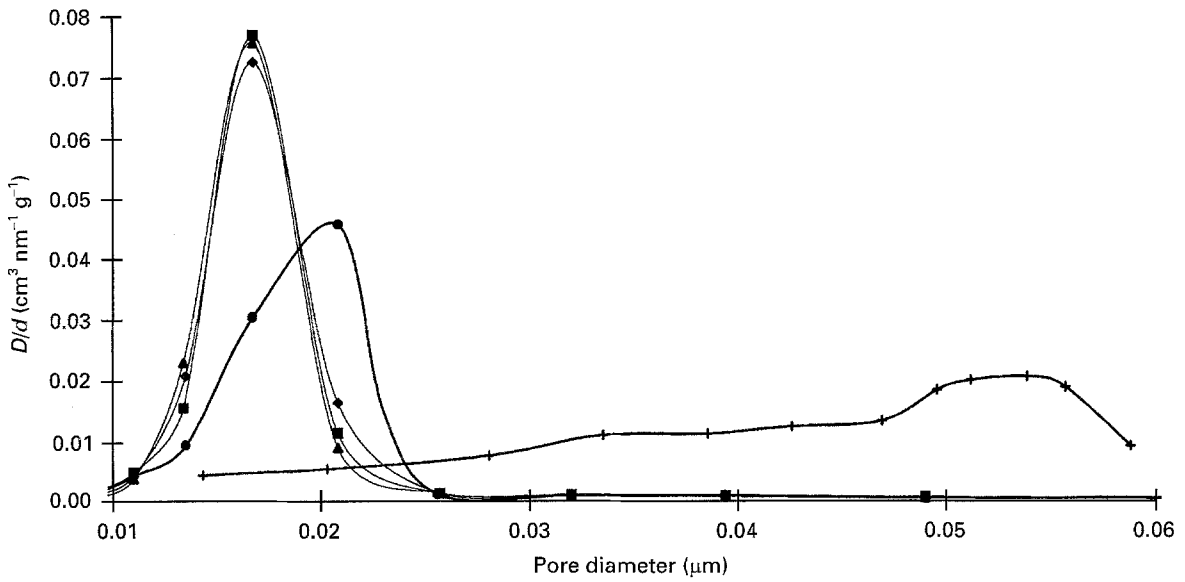

Figure 2 Pore-size distribution of differently processed ultrafine SiC powders: (▲) uniaxially pressed, (■) H_2O, (◆) H_2O freeze dried, (●) ethanol, (+) SiCB20 ethanol.

TABLE II Characterization of ultrafine SiC powders processed by different methods (see text)

Powder processing	Before CIP		After CIP			
	Caron content (wt%)	Oxygen content (wt %)	Av. pore diameter (nm)	Total pore area ($m^2 g^{-1}$)	(Apparent) density ($g\ cm^{-3}$)/%TD	Density geometrical ($g\ cm^{-3}$)/%TD
Cold isostatically pressed	29.9/–/24.8	1.36/–/1.72	18.6	97.2	1.23 (2.79)/38.3	1.22 ± 0.07/38.0
Water	29.8/29.6/29.1	1.93/1.94/1.92	18.7	97.2	1.22 (2.72)/38.0	1.12 ± 0.03/34.9
Water freeze dried	29.8/29.9/28.4	1.36/1.94/1.87	18.6	99.1	1.25 (2.98)/38.9	1.14 ± 0.03/35.5
Ethanol	28.1/29.8/29.2	–/–/1.99	21.7	77.1	1.34 (3.07)/41.7	1.36 ± 0.04/42.3

other methods. One explanation might be the low surface tension of ethanol which leads to reduced pressures during drying and therefore to a more open, loosely packed microstructure. On the other hand, the agglomerates formed during drying are relatively soft. During pressing they will easily break and therefore an increased green density will result.

If the mean pore diameters are compared with the particle size (15 nm) it is found that the pore size is larger than the particle size. This indicates an open structure in which interagglomerate pores, as described elsewhere [9], also play an important role.

As can be seen from the sintering results, these microstructures lead to extensive grain growth if pressureless sintering is applied. It is also shown below that hot isostatic pressing can effectively reduce the mean pore diameter.

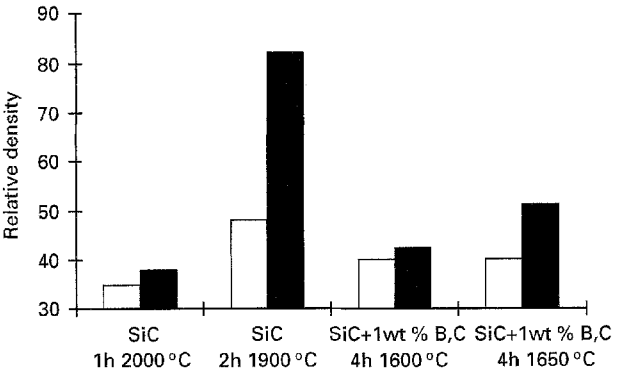

Figure 3 (□) Green densities and (■) final densities after pressureless sintering of ultrafine SiC powders with and without sintering agents.

3.2. Pressureless sintering

Results of pressureless sintering of specimens with 1 wt % boron and carbon addition using ethanol as a solvent, are given in Fig. 3. Also included are results of cold isostatically pressed ultrafine SiC powders without sintering agents. The high green density (48% theoretical) of one of the samples was achieved by milling the powders in a planetary mill before cold isostatic pressing. Specimens without sintering agents were not treated for the whole time under argon. Therefore their oxygen content before sintering (5 wt %) was higher than that of the samples with sintering agents (see Table I). During sintering, the oxygen content decreases below 1.5 wt % (0.08 wt % in the case of the sample sintered at 2000 °C) probably

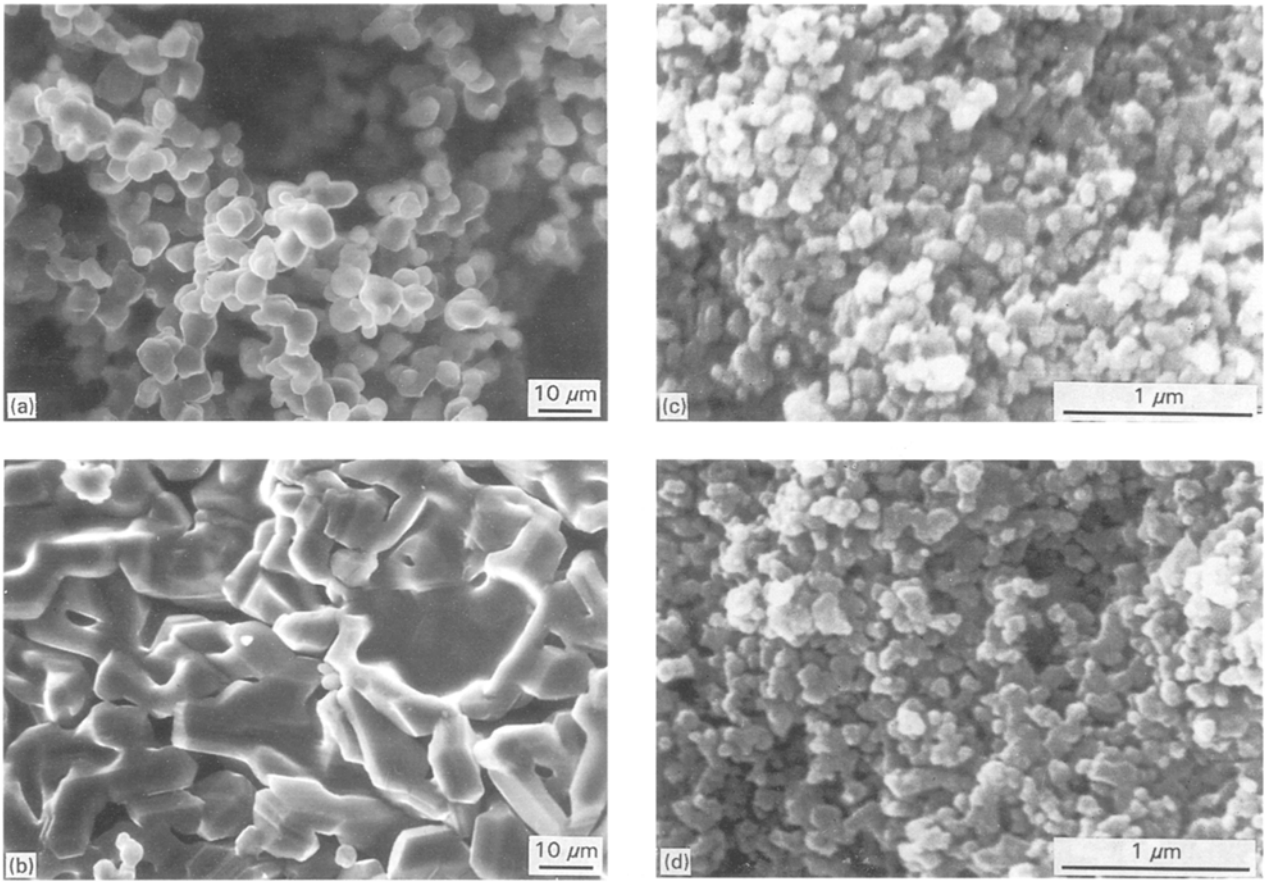

Figure 4 Scanning electron micrographs of sintered ultrafine SiC. (a)–(d) correspond to the samples in Fig. 3 from right to left.

due to reaction of SiO_2 with carbon from the graphite furnace.

The sample with sintering agent shows a significant density increase at 1650 °C, although the final density is still low. Densification of the specimens without sintering agents starts at considerably higher temperatures (> 1850 °C), which was confirmed by dilatometric measurements [22]. Furthermore, comparison of the densities of the samples without sintering agents indicates the large effect of green density on the densification. This is also demonstrated by the micrographs given in Fig. 4. The specimen without sintering agents and with low green density (Fig. 4a) after sintering for 1 h at 2000 °C, revealed a microstructure which was very similar to the laser-synthesized starting powder (Fig. 1a). The major difference is the scale; the "particles" grew by more than two orders of magnitude to a grain size of about 5 μm. Also, the sample without sintering agents and high green density (Fig. 4b) revealed large grain growth (10 μm). But in this case, a much lower porosity level was also observed.

Fig. 4c and d show samples with sintering agents sintered at 1600 and 1650 °C, respectively. Grain sizes were estimated to be approximately 62 and 74 nm. The factor of 1.2 (see Section 2.2) has not been taken into account because the particles are isolated and not embedded in a matrix.

The coarsening of the microstructure during sintering was also found in porosity measurements (Fig. 5). The mean pore size of a sample sintered at 1600 and 1650 °C increases from about 20 nm in the green state to about 63 and 76 nm, respectively, after sintering. Kingery and Francois [23] showed that for a given dihedral angle, ϕ, there exists a critical ratio of pore size to particle size. If this value is exceeded, pores will grow. The dihedral angle of SiC can be estimated using a grain boundary energy, γ_{gb}, of 2.5 $J m^{-2}$ [24], a surface energy, γ_s, of 1.85 $J m^{-2}$ [13] and applying

$$\cos\left(\frac{\phi}{2}\right) = \frac{\gamma_{gb}}{2\gamma_s} \quad (1)$$

The value ϕ of 95° is close to the result (92°) reported elsewhere [25]. It corresponds to a maximum pore size to grain size ratio of 0.5 [23]. Taking the powder particle diameter of 15 nm and the pore sizes given in Table II, ratios between 1.24 and 1.46 were obtained for our samples. Even if a reduction of the grain-boundary energy due to the segregation of boron and an increase of surface energy due to the reduction of SiO_2 by the added carbon, leads to an increase of the dihedral angle [11], a densification of loosely packed ultrafine SiC without excessive grain growth is difficult, as observed in the present experiments. Sintering at 1650 °C led to a reduction of the pore size to grain size ratio to a value of about 1 (Table III) which is still much larger than the maximum value for pore shrinkage. So further pore growth is expected during subsequent sintering.

As shown in Table IV, similar results on the sintering of ultrafine SiC powders have been found by other

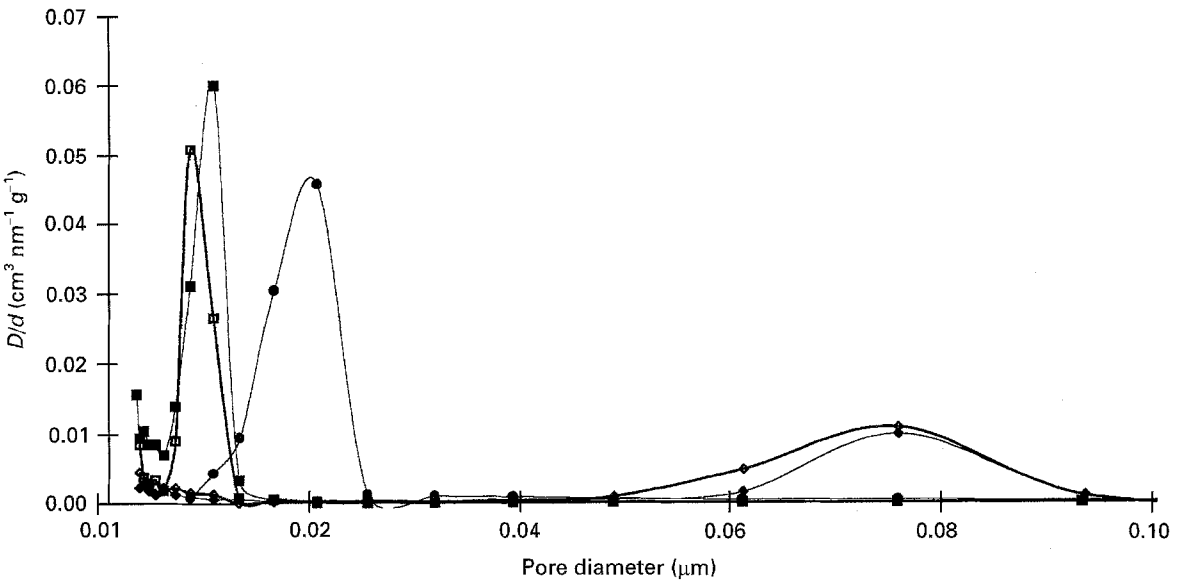

Figure 5 Pore-size distribution of green, sintered, and HIPed samples prepared from ultrafine SiC powder with 1 wt % boron and carbon addition. (□) One sample HIPed at 1150 °C contained no sintering additive. (●) SiC ethanol; (◇) sintered 1600 °C, SiC + B, C; (◆) sintered 1650 °C, SiC + B, C; (■) HIP 1150 °C, SiC + B, C.

TABLE III Results of porosity measurements of green bodies, sintered, and HIPed specimens

Sample	Av. pore diameter (nm)	Total pore area ($m^2 g^{-1}$)	Apparent density ($g cm^{-3}$)	Density Hg-poros ($g cm^{-3}$)/%TD
Green body[a]	21.7	77.1	2.96	1.34/41.7
Sintered at 1600 °C, 4 h[a]	62.5	17.6	3.33	1.74/54
Sintered at 1650 °C, 4 h[a]	75.7	10.9	3.59	2.07/64
HIPed at 1150 °C, 300 MPa, 3 h	10.2	66.9	2.85	1.92/59.8
HIPed at 1150 °C, 300 MPa, 3 h[a]	10.9	70.7	2.42	1.65/51.4

[a] Sintering additives used (1 wt % B, C).

authors. Pressureless sintering of SiC to densities beyond 90% theoretical without excessive grain growth has not, to our knowledge, been stated in the literature up to now. The relatively small grain sizes and large densities of sintered SiC powders [26] are probably due to the achieved high green densities of about 70% theoretical by uniaxial pressing of small pellets with pressures of 2 GPa. But this method is not suitable for the production of larger ceramic parts.

3.3. Hot isostatic pressing (HIPing)

3.3.1. Results on densification

The following figures give an overview of the influence of different parameters such as powder processing, temperature, pressure, dwell time, sintering additive content and amount of conventional powders on the HIP densification of ultrafine and, for comparison, conventional SiC powder. Green bodies produced from differently processed powders (Table II) were HIPed at 1700 °C and 350 MPa for 20 min. The results are summarized in Table V. They indicate that powders processed with ethanol give the highest densities with grain sizes close to the samples prepared by mixing with water. As a result, further experiments were performed using processing with ethanol.

In Fig. 6 the final densities of ultrafine SiC powders with and without sintering additives after HIPing at different temperatures are given. Unless stated otherwise, HIPing dwell time varied between 3 and 4 h. The sample SiC with 1 wt % B and C HIPed at 1500 °C was held for 5 h at the maximum pressure. Also results for shorter HIP cycles are given (indicated as 10–20 min, 20 min at 1700 °C, 10 min at 1800 and 1900 °C). For comparison, the densification behaviour of conventional powder (HC Starck B20) is also shown. Doped ultrafine powders achieve densities of 3.05 $g cm^{-3}$ (95% theoretical) and above, at temperatures between 1500 and 1600 °C, whereas the densities of samples made of conventional and undoped ultrafine powders do not exceed 2.89 $g cm^{-3}$ (90% theoretical) below 1650 °C. Doped and undoped conventional powders show no significant difference.

Fig. 6 also reveals the influence of the amount of sintering agent and the method of mixing it: SiC + B + C or SiCB + C powder mixed with ethanol in a turbula mixer (see Section 2.1). Unfortunately, the sintering agent contents are not exactly the same, but nevertheless some general tendencies can be found. Firstly, there seems to be no significant difference between conventional mixing and mixing during the laser synthesis. Secondly, an increasing amount of

TABLE IV Results given in the literature on the sintering of ultrafine SiC powders

Reference	Powder characteristics	Sintering temperature (°C)	Approx. grain size (μm)	Density (% TD)
Nannetti *et al.* [45]	Laser synthesized + B, C; ≈ 20 nm	2000–2050	> 1	96
Baumgartner *et al.* [46]	Plasma synthesized SiC + B, C; 200–500 nm	2025–2175	10 to > 100	94–98
Kijima *et al.* [43]	Plasma synthesized SiC; 5 nm	1900–2300	≈ 1 (?)	67–87
Croix *et al.* [42]	Laser synthesized SiC + B, C; 15–30 nm	1800–2100	0.4	70–96
Wehling [47]	Plasma synthesized SiC + B, C; ≈ 150 nm	2100	8	94–97
Bishop *et al.* [48]	Polymeric precursor SiC + 19 wt % excess C + B_4C, 3 nm (XRD)	1900–2100	0.5–2	70–93
Ohkohchi *et al.* [49]	Gas evaporation SiC + 15 wt % excess Si; carbon substrate; 50 nm	1550–2200	Excessive grain growth	Low
Vaßen [26]	Laser-synthesized + 50 wt % excess Si; 14 nm	1050–1500	< 0.1	75–88

TABLE V Densities and grain size of samples processed with water or ethanol and HIPed at 1700 °C for 20 min with a pressure of 350 MPa

Powder processing	Density (%TD)	d_{SEM} (nm)
Water	89.2 ± 0.9	309 ± 20
Water freeze dried	90.3 ± 1.3	390 ± 32
Ethanol	91.4 ± 3.2	350 ± 30

sintering agent (B + C) leads to a reduction of the final density.

In Fig. 7a, the pressure dependence of the final density is shown for different powders and different HIPing temperatures. The values at 350 MPa and 1550 °C were calculated by taking the mean densities of two samples HIPed at the given pressure at 1500 and 1600 °C. With the exception of a slight decrease of the doped conventional SiC, there is a general increase in density with HIP pressure.

In Fig. 7b the influence of the dwell time on the final density is shown for two HIP runs, both performed at 1600 °C. Taking into account the difference in HIP pressures, which would slightly increase the slope of the data points (40 MPa corresponds to 2% theoretical density (TD) = 0.064 g cm^{-3} according to a mean pressure dependence of 0.05% TD/MPa taken from Fig. 7a), the slope of the data points of ultrafine powders is about 1.7% ± 0.7% TD/h and is similar to the results of Gilissen *et al.* (1.4% TD/h [27]), which are also included in Fig. 7b. Often the potential of ultrafine powders as sintering agents is discussed. To investigate this application, two types of conventional powders were mixed with ultrafine SiC powders (+ B, C) and HIPed. The results are shown in Fig. 8. Obviously the density increases nearly linearly with increasing ultrafine powder content. As a result, the increase for low amounts of ultrafine powder is only marginal and

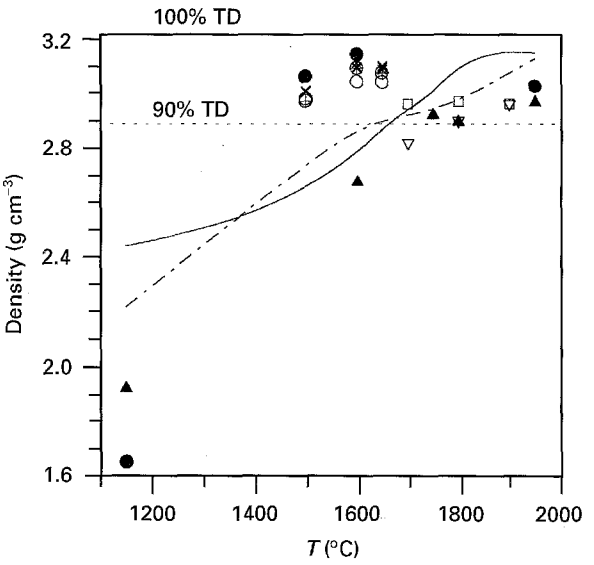

Figure 6 Densities of ultrafine (●, ×, □, ▲, ▽) SiC and (⊕, ○) SiCB powders after HIPing at the given temperatures for 3–4 h at 350 MPa (300 MPa at 1150 °C), doped (▲, ⊕, ▽ (10–20 min)) without and with (●, □ (10–20 min)), 1 wt % or (○ (C), ×) 2.5 wt % carbon and boron. For comparison, the densities of conventional powders (HCS = B20 from HC Starck, particle size ≈ 500 nm) are also shown: (— · —) HCS + 1 wt % B, C, (——) HCS.

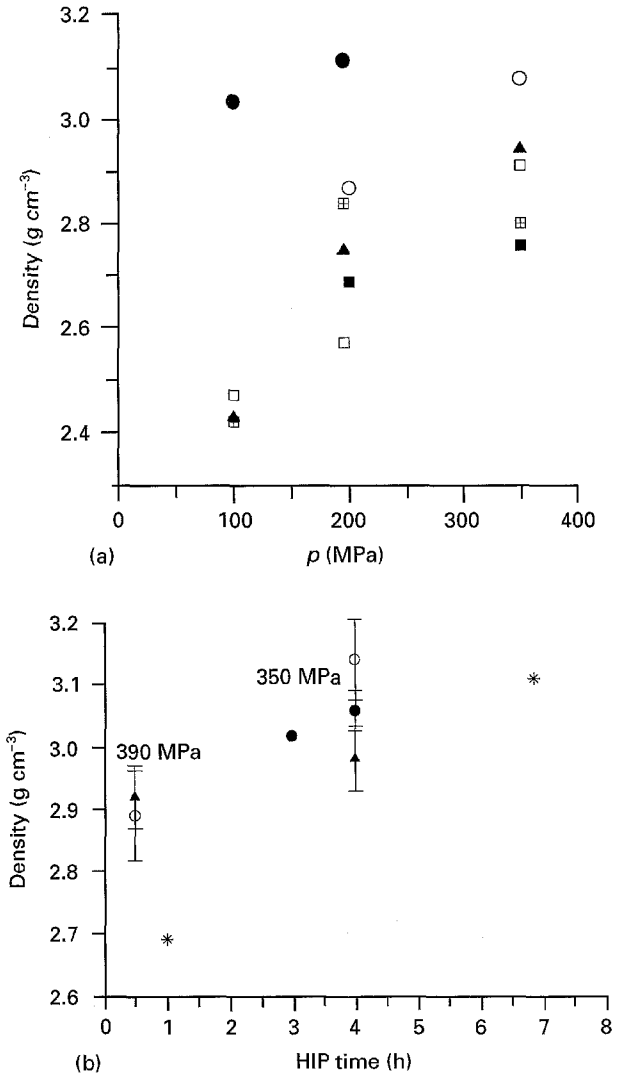

Figure 7 Dependence of the relative densities of HIPed ultrafine SiC powders on (a) HIP pressure and (b) HIP time. (a) (○) Nano + B + C, 1550 °C (cal); (●) nano + B + C, 1680 °C; (▲) nano + HCS + B, C, 1680 °C; (■) HCS + B, C, 1550 °C (cal); (⊞) HCS + B, C, 1680 °C; (□) HCS 1680 °C. Nano corresponds to the ultrafine SiC powder while HCS indicates a conventional SiC powder produced by HC Starck. (b) (●) SiC + B, C, 1500 °C; (○) SiC + B, C, 1600 °C; (▲) SiC + HCS + B, C, 1600 °C. A result from Gilissen *et al.* [27] is also given (*).

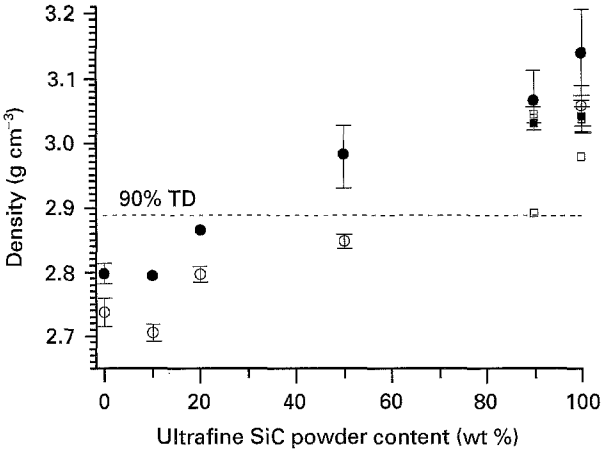

Figure 8 Influence of the amount of ultrafine powders on the density of ultrafine/conventional powder mixtures. (○) SiC + 1 wt % B, C, 1500 °C; (●) SiC + 1 wt % B, C, 1600 °C; (□) SiCB + 2.5 wt % C, 1500 °C; (■) SiCB + 2.5 wt % C, 1600 °C; (⊞) SiCB + 2.5 wt % C, 1650 °C.

TABLE VI Results of chemical analysis and grain-size determination of green bodies, sintered, and HIPed specimens

Sample	Carbon content (wt %)	Oxygen content (wt %)	d_{SEM} (nm)	d_{XRD} (nm)
Green body[a]	30.0	2.0	15[b]	3–5
Sintered at 1600 °C, 4 h[a]	–	–	62 ± 4	–
Sintered at 1650 °C, 4 h[a]	30.7	1.3	74 ± 5	–
HIPed at 1150 °C, 300 MPa, 3 h	30.7	3.7	51 ± 4	5.9 ± 0.4
HIPed at 1150 °C, 300 MPa, 3 h[a]	30.5	3.4	58 ± 4	4.5 ± 0.1
HIPed at 1700 °C, 350 MPa, 20 min	29.5	2.3	74 ± 14	29 ± 4
HIPed at 1700 °C, 350 MPa, 20 min[a]	29.7	3.4	360 ± 32	> 100

[a] Sintering additives used (1 wt % B, C). [b] Particle size determined by TEM.

so ultrafine SiC powder does not act as a sintering agent in the sense that small amounts lead to significant increase in density. On the other hand, mixtures of ultrafine powders with rather small amounts (e.g. 10 wt %) of conventional coarse-grained powders, can be densified at rather low temperatures. This type of ceramic offers promising mechanical properties [7].

3.3.2. Characterization of HIPed samples

3.3.2.1. Chemical analysis. Results of chemical analysis of several HIPed and also sintered specimens are given in Table VI. The amount of oxygen lies in the range between 2.3 and 3.7 wt %, the carbon content is close to the stoichiometric carbon content in SiC (30 wt %). A slightly lower oxygen content in doped specimens compared to undoped samples was found at 1150 °C, while a higher content was found after HIPing at 1700 °C. An effective reduction of the surface oxygen on the SiC powder is prevented by the cladding of the samples. This is confirmed by the comparison with the sintered specimen which shows a significantly lower oxygen content.

The oxygen content in the HIPed specimens leads to a reduction of the density compared to oxygen-free SiC. Assuming densities of 2.20 g cm^{-3} for SiO_2 and 3.21 g cm^{-3} for SiC, the theoretical density of the HIPed specimens with oxygen contents between 2.0 and 3.7 wt % lies between 3.11 and 3.15 g cm^{-3}. A further reduction of the theoretical density is caused by excess carbon. For the HIPed sample with a low amount of carbon (29.5 wt %), an amount of 1.1 wt % carbon is calculated if it is assumed that only SiC, C, and SiO_2 are present in the sample. This amount results in a theoretical density of about 3.13 g cm^{-3}, with taking 2.25 g cm^{-3} as the theoretical density of the used carbon.

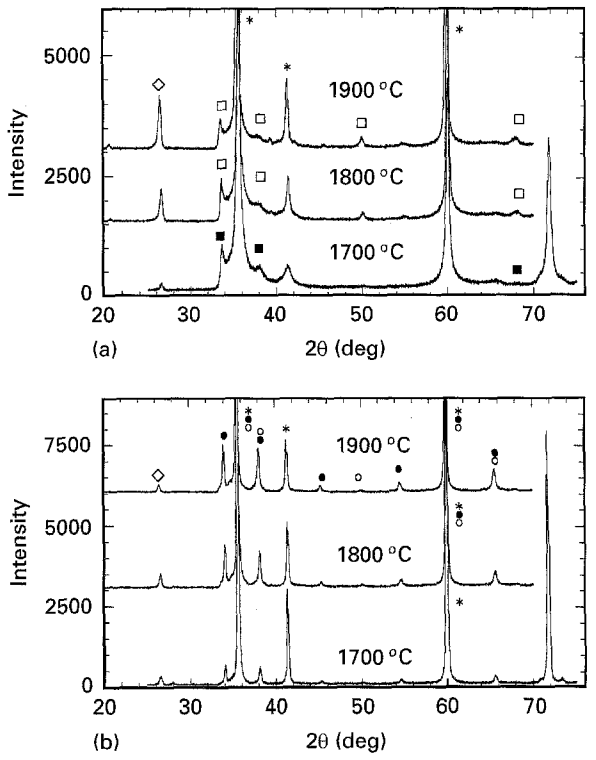

Figure 9 XRD results of SiC specimens prepared from (a) undoped and (b) doped (1 wt % B, C) ultrafine SiC powders HIPed at the given temperatures for 10 min (1800 and 1900 °C) and 20 min (1700 °C) at 350 MPa. (*) SiC-3C, (□) 2H, (●) 6H, (○) 4H, (◇) SiO_2.

As a result of this evaluation, it is clear that the highest densities achieved by HIPing (Fig. 6) are closed to the theoretical density (> 99% theoretical). Also the reduction of density in the samples with higher amounts of sintering additives can be explained by the higher amount of excess carbon.

3.3.2.2. Phase analysis. In Fig. 9 the results of XRD measurements of doped and undoped samples HIPed at 1700, 1800, and 1900 °C for dwell times between 10 and 20 min are given. It is clearly visible that the undoped samples show much broader peaks, indicating smaller grain sizes (see also 1700 °C run in Table VI).

The amount of β-SiC, the low-temperature cubic (zinc blende) modification, is larger in the undoped material. The high-temperature α-SiC is only present as the hexagonal 2H modification (wurzite). In the doped material, the 4H and 6H and, above 1800 °C, small amounts of the rhomboedric 15R modifications (not visible in Fig. 9), are also present, while the 2H peaks are missing. XRD measurements on doped specimens HIPed at lower temperatures for longer dwell times (3–4 h) gave results which were similar to the results of the doped specimens given here. A detailed discussion can be found elsewhere [15].

Doped and undoped samples with comparable grain size (e.g. 250 nm for an undoped sample HIPed at 1900 °C and a doped sample HIPed at 1500 °C, see below) show the same difference. Consequently, the additives seems to promote the formation of 4H and 6H modifications. A possible explanation might be that the boron atoms lead to the easy introduction of stacking faults into the SiC. This results in the formation of the mentioned polytypes [28].

3.3.2.3. Grain size. Grain size is one characteristic feature of nanocrystalline materials. Therefore, a comparison of different methods of grain-size analysis has been performed by investigating one sample using TEM, SEM, and XRD. One sample was prepared from ultrafine SiC with 1 wt % B and C addition and HIPed at 1680 °C with a pressure of 100 MPa. The final density was 3.03 $g\,cm^{-3}$ and the oxygen content was 6.3 wt %. This high oxygen content was due to the fact that the sample was produced before all the processing steps were performed under argon. As seen above, the oxygen contents of samples handled under inert gas are significantly lower. A transmission electron micrograph of the sample is given in Fig. 10a. It reveals a broad grain-size distribution from 200–1000 nm with a mean value of about 490 ± 60 nm. This value corresponds reasonably well with SEM results from an investigation of a fracture surface (360 ± 70 nm). XRD analysis (mean value of the Scherrer formula applied to the (1 1 1), (2 0 0), (2 2 0), and (3 1 1) peaks) gave grain sizes of 48 ± 8 nm. This value is considerably lower than the grain sizes found by SEM and TEM. In Fig. 10a and b, many stacking faults or twinning boundaries are visible. As a result, the size of the area of coherent scattering is reduced to 50–200 nm (Fig. 10b), which corresponds fairly well with the XRD results. It is interesting to mention that the ratio of TEM and SEM to XRD grain size is about 4 in the powder, while it varies from a factor of 4 to 10 in the densified material (Table VI).

The high number of twinning boundaries and stacking faults, which was already mentioned in the discussion of the XRD results, is also reported in the literature for sintered fine-grained Si and SiC materials [10, 11, 29] and has been found especially during the β–α transformation in conventional SiC ceramics [30]. These two-dimensional defects have a lower interfacial energy compared to high-angle grain boundaries, and also the mobility in these interfaces is lower. Therefore, the size of coherent scattering regions, as determined by XRD, is not necessarily equal to the grain size of nanophase materials in the sense of Gleiter [31].

In Fig. 5 the porosity distributions of specimens HIPed at 1150 °C are compared to those in sintered and green bodies. It is found that the mean pore diameter as well as the pore volume is reduced by HIPing (see Table III) while the total pore area is only slightly reduced. Consequently, HIP densification at these low temperatures takes place without significant coarsening. To achieve similar densities by sintering, considerably higher temperatures have to be used. Densification is then followed by an enhanced coarsening of the microstructure. SEM investigations on the samples HIPed at 1150 °C also reveal a fine-grained microstructure (Fig. 11). Owing to the low density of the samples and the resulting open structure it seems to be reasonable to leave the factor 1.2 (see Section 2) when determining the grain size from scanning

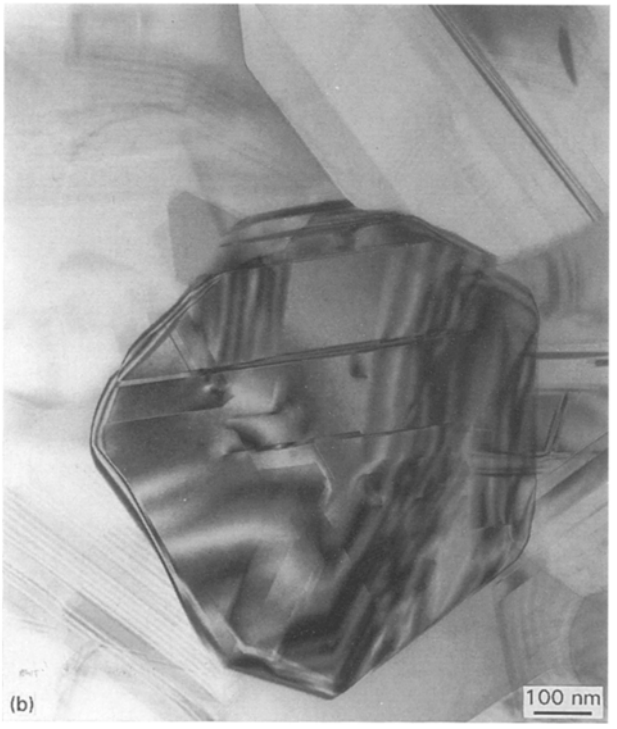

Figure 10 Transmission electron micrographs of a SiC sample prepared by HIPing ultrafine SiC powder with 1 wt % boron and carbon addition at 1680 °C. (a) An overview of the sample, (b) the high amount of stacking faults and twinning boundaries revealed within an individual grain.

electron micrographs. The grain sizes of the samples with and without sintering additives are then approximately 42 and 39 nm, respectively. Owing to the limited resolution of the SEM it is possible that actual grain size is even smaller.

3.3.3. Grain growth and densification results

In Fig. 12, results of grain sizes of several HIPed samples determined by SEM are plotted against the

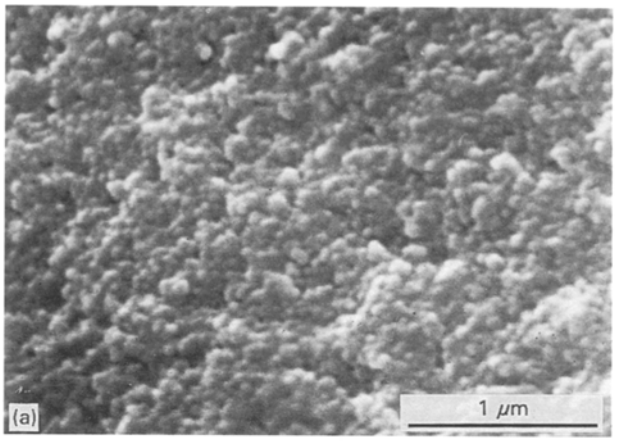

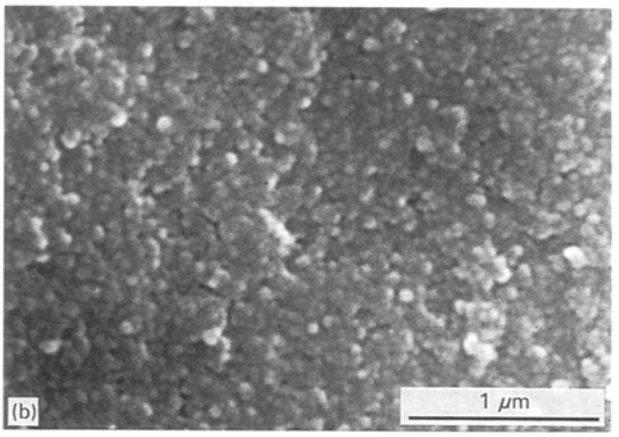

Figure 11 Scanning electron micrographs of SiC samples (a) with and (b) without 1 wt % B, C HIPed at 1150 °C and 300 MPa for 3 h.

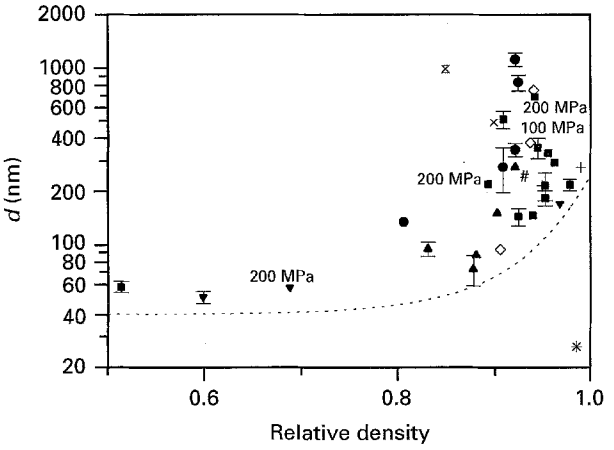

Figure 12 Present results on HIP densification of (●, ■) doped and (▼, ▲) undoped ultrafine SiC powders. Short cycles (●, ▲) have been performed with dwell times between 10 and 30 min, while in the other experiments dwell times between 3 and 5 h were used. Literature results on the pressure-assisted densification of, in one case, Si_3N_4, and of SiC powders are also given: (×) Si_3N_4, 1900 °C, HIP 198 MPa, 1 h [12], (+) SiC + 1.4% Al, 1800 °C, HP 50 MPa, 1–3.5 h [29]; (#) SiC + B, 1900 °C, HP, 1 h [42]; (⧖) SiC, 2200 °C, HP 40 MPa, 0.5 h [43]; (◇) SiC + B, C, 1500–1600 °C, HIP 195 MPa, 1 h [27]; (*) SiC in Si_3N_4, 1800 °C, 350 MPa 3 h [44]. (- - -) The lowest achieved grain size for a given density.

achieved densities. Different ways to increase the density and to reduce grain size have been investigated. HIPing without sintering additives leads to reduced grain growth but also to reduced densities at the same HIP temperature. Similar densities are achieved at

about 200 °C higher temperatures (see Fig. 6). Samples with carbon but no boron additives show a behaviour similar to the samples without additives (results not given here). In SiC samples without sintering agents which, at temperatures above 1650 °C, reach densities of 90% theoretical, considerable grain growth is also observed.

A comparison of the results of long-term HIPing of ultrafine SiC samples with and without sintering agents reveals only slight differences between both kinds of samples. At low densities, grain growth seems to be reduced in the case of undoped powders. This would be more obvious if the data point at 2.2 g cm^{-3} (69% TD, 200 MPa HIP pressure) is moved to higher densities to compare it with the results after HIPing at 350 MPa.

Reducing the dwell time and increasing the temperature for samples with sintering additives led to lower densities as compared to samples with comparable grain sizes HIPed at longer times. Samples without sintering agents show a very fine grain size at densities of about 90% theoretical. Higher densities also led to intense grain growth but grain sizes are still finer than in samples with sintering additives and comparable densities.

For comparison, data from pressure-assisted sintering of SiC and Si_3N_4 presented by other authors are also given in Fig. 12. To our knowledge, at present it is not possible to produce dense monoclinic SiC ceramics with grain sizes lower than the enveloping curve given in Fig. 12. On the other hand, if SiC is embedded in a different matrix (e.g. Si_3N_4 (*)) finer grain sizes can be easily obtained owing to an effective separation of the SiC grains.

A similar mechanism operates during the HIPing of ultrafine SiC powders annealed in nitrogen. Owing to the formation of a Si_3N_4 layer on the powder surface, these powders show, compared to non-treated powders, significantly reduced grain growth rates [32].

3.3.4. Modelling

In the following section an attempt is made to develop a densification model which is able to explain our experimental results.

3.3.4.1. Grain growth. Owing to the significant grain growth which takes place during densification, it is necessary to introduce this coarsening process into the densification model. Therefore, an analytical description of the grain growth has to be found. The comparison of the results with models given in the literature might also lead to identification of the grain growth process. Knowledge of the relevant coarsening processes can be an important help to minimize grain growth by an adequate choice of the densification parameters. Often grain growth can be described by the following equation [33]

$$d^n - d_0^n = C\,t \qquad (2)$$

in which $d\,(d_0)$ is the (initial) grain size, and t the time, n is a constant depending on the mechanism and

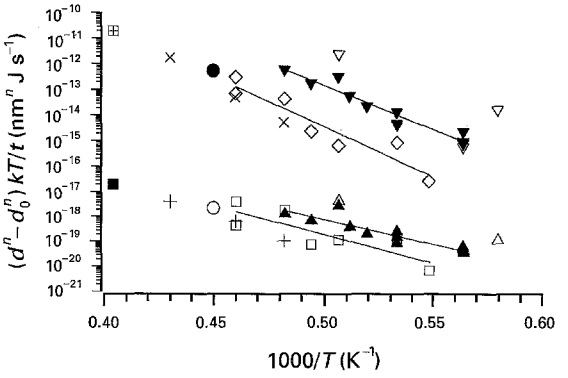

Figure 13 $(d^n - d_0^n)kT/t$ plotted over the inverse temperature. (——) square fits (see text and Table VII). SiC + B, C (▲) $n = 2$, (▼) $n = 4$. SiC (□) $n = 2$, (◇) $n = 4$. (+) SiC + Al (N), $n = 2$ [29]; (×) SiC + Al (N), $n = 4$ [29]; (○) Si_3N_4, $n = 2$ [12]; (●) Si_3N_4, $n = 4$ [12]; (■) SiC, $n = 2$ [43]; (⊞) SiC, $n = 4$ [43]; (△) SiC + B, C, $n = 2$ [27]; (▽) SiC + B, C, $n = 4$ [27].

usually between 2 and 4. The constant C is proportional to the diffusion coefficient of the operative mechanism divided by kT, i.e. C has the form $C = C_0\exp(-U/kT)/kT$, U being the activation energy of the operating mechanism. There are insufficient isothermal data points to determine the constant n separately. Therefore $\ln(d^n - d_0^n)kT/t$ was calculated for all specimens with densities above 90% theoretical ($d_0 = 15$ nm) and a least square fit of the inverse temperature dependence was made. The results are shown in Table VII. For $n = 2$ and 4 the results are also plotted in Fig. 13.

The results in Table VII show an increasing correlation coefficient with increasing n. A coefficient of $n = 4$ would indicate grain growth controlled by pore movement via surface diffusion [26, 33]. In this case, the factor C_0 has the form

$$C_0 = \alpha\left(\frac{d}{d_{\mathrm{pore}}}\right)^4 \gamma_{\mathrm{gb}}\Omega^{\frac{4}{3}}D_{\mathrm{so}} \qquad (3)$$

with d/d_{pore} being the grain to pore diameter ratio (assumed to be constant), D_{so} the prefactor of the surface diffusion coefficient, γ_{gb} the grain-boundary energy, Ω is the atomic volume, and α a constant of the order of 1. For this mechanism, the activation energies of doped (6.8 ± 0.7 eV) and undoped (7.7 ± 1.2 eV) samples are similar within the experimental error. These values are between the measured values of the activation energy of a grain boundary (3.1–6.2 eV, ^{14}C in SiC [34]) and volume diffusion (7.2–9.5 eV for ^{30}Si [35, 36] and 7.4–8.7 eV for ^{14}C [37, 38] in SiC). The same is true for the absolute values of the diffusion coefficients if a value of 10 is assumed for d/d_{pore}. For surface diffusion, a lower activation energy and a higher absolute value are expected but, on the other hand, no data on surface diffusion on SiC have been found to verify this statement. If grain growth is controlled by pore movement via surface diffusion, the difference between doped and undoped samples, i.e. grain size is significantly smaller in the case of undoped samples, must also be explained. In terms of the proposed grain-growth kinetics (Equation 2) this indicates that the factor C_0 (Equation 3) is lower in the case of

TABLE VII Results of least square fits of the inverse temperature (1000/T(K)) dependence of $\ln(d^n - d_0^n)kT/t$

Specimens	n	C_0 ($m^n J^{-1} s$)	U (eV)	Correlation coefficient
SiC + B, C	2	6.52×10^{-27}	3.86 ± 0.61	0.816
SiC + B, C	3	1.82×10^{-29}	5.33 ± 0.59	0.902
SiC + B, C	4	5.26×10^{-32}	6.80 ± 0.65	0.923
SiC + B, C	5	1.52×10^{-34}	8.28 ± 0.79	0.924
SiC + B, C	6	4.41×10^{-37}	9.75 ± 0.97	0.918
SiC	2	5.61×10^{-26}	4.47 ± 1.27	0.712
SiC	3	1.15×10^{-28}	6.08 ± 1.20	0.837
SiC	4	2.67×10^{-31}	7.73 ± 1.21	0.891
SiC	5	6.32×10^{-34}	9.37 ± 1.29	0.913
SiC	6	1.51×10^{-36}	11.01 ± 1.44	0.921

undoped samples, i.e. the pore diameter is larger and/or the grain-boundary energy smaller. On the contrary, as mentioned above, the grain-boundary energy should be smaller for the doped samples, and the porosity measurement given in Fig. 5 also reveals the opposite tendency for the pore diameter.

A possible explanation might be the fact that densification and grain growth are both present during HIPing. However, the deduced law for pore-controlled grain growth assumes no change in the porosity level. Especially in the case of the undoped samples, this may affect the grain growth results because these samples have, on average, a lower density than the doped samples.

If pore movement via volume diffusion is assumed, the exponent $n = 3$ is expected [33]. The major change in the factor C_0 is the change of the exponents 4 to 3. The resultant activation energies (Table VII, $n = 3$) are far below the values given above and the absolute values are larger than expected. Also the correlation coefficient drops considerably (Table VII). We therefore assume that $n = 4$ is a more reasonable description of the grain-growth process and the growth law is integrated into the densification model described below.

3.3.4.2. HIP densification. The description of the HIP densification is mainly based on formulas given elsewhere [39]. Matter is assumed to be transported by diffusion. Then, in the initial stage (< 90% TD), the following densification rate is found

$$\frac{d\rho}{dt} = \frac{96\rho^2}{\rho_{gr} d^3 g(\rho)} \frac{\delta D_{gb} + \varepsilon D_{vol}}{kT} \Omega Z p^* \quad (4)$$

where $g(r)$ is a geometrical term which ranges from 0.76 at the green density (0.64 assumed for random dense packing) to 2.12 at 90% TD, $\rho_{(gr)}$ is the (green) density, δ the grain-boundary width, D_{gb} and D_{vol} the grain-boundary and volume-diffusion coefficient, Z is the number of particle contacts (values between 7 and 10), and p^* is the effective pressure

$$p^* = \gamma_s \left(\frac{1}{\varepsilon} - \frac{2}{x} \right) \quad (5a)$$

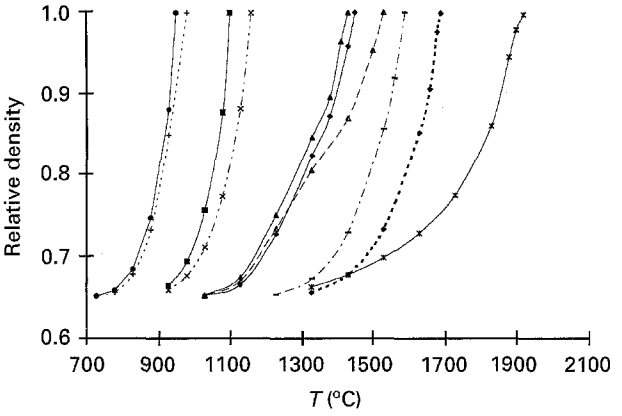

Figure 14 Results of the HIP modelling described in the text. The parameters used are given in Table VIII. Other parameters used are as in the key. (●) 6.23 eV; (+) 6.23 eV, p HIP = 0 MPa; (×) 6.23 eV, d = 200 nm; (■) 7 eV; (▲) 8 eV; (△) 8 eV, p HIP = 0 MPa; (◆) 8 eV, t HIP = 1 h; (−) 8 eV, d = 200 nm; (◇) 8 eV, d = 500 nm, (*) 9 eV.

and

$$\varepsilon = \frac{x^2}{4(d - x)} \quad (5b)$$

with x being the neck diameter.

For the final-stage sintering (> 90% TD) the following equation was used

$$\frac{d\rho}{dt} = \frac{162\rho^2}{d^3 f(\rho)} \frac{\delta D_{gb} + r D_{vol}}{kT} \Omega \left(p + \frac{2\gamma_{gb}}{r} \right) \quad (6)$$

where $f(\rho)$ is a geometrical term which increases slowly with density from 0.6 at 90% TD to 4 at 99.9% TD.

As mentioned above, the grain size was calculated using the parameters for SiC with sintering additives in Table VII for $n = 4$. A similar procedure for copper powders and a parabolic growth law is described elsewhere [40].

In Fig. 14 the results of the HIP modelling for standard parameters given in the literature (see Table VIII) are shown. Densification should start at about 1000 °C, which is about 500 °C lower than observed in our experimental results (Fig. 6). Even without applying a HIP pressure, the sintering behaviour remains nearly unchanged. This can be explained by

TABLE VIII Parameters used in the HIP modelling

U_{gb} (eV)	D_{gb0} ($m^2 s^{-1}$)	U_{vol} (eV)	D_{vol0} ($m^2 s^{-1}$)	t_{HIP} (10^3 s)	p_{HIP} (MPa)	δ (nm)	γ_s ($N m^{-1}$)	Ω (m^3)	d (nm)
6.23	1.38×10^4	9.45	8360	10.8	350	10^{-9}	1.85	10^{-29}	1.6×10^{-8}

the fact that according to our model, grain growth does not occur at 1000 °C. So the sintering pressure, $2\gamma/r$, remains extremely large during the whole sintering. This observation might lead to the assumption that the beginning of the grain-growth process might not be adequately described by the $t^{1/4}$ law given in Equation 2. There might be a very fast grain growth even at low temperatures, e.g. due to dislocation movement [41]. The increased grain sizes found after HIPing at 1100 °C (Table VI) might indicate such a behaviour. Therefore, the densification of SiC with starting grain sizes of 200 nm has also been calculated. But even a grain size of 200 nm results in high densities at 1100 °C (Fig. 14), which were not found in our experiments.

Consistent results can be obtained if the grain-boundary diffusion coefficient is decreased, which was done by increasing the activation energy and leaving the prefactor constant. Decreasing the volume diffusion coefficient has no effect because densification via volume diffusion is, according to our model, negligible below 2000 °C.

Fig. 14 shows that an activation energy for grain-boundary diffusion of 8 eV leads to full density after HIPing for 3 h with 350 MPa, at about 1430 °C which is in reasonable accordance with our experimental results.

A similar activation energy was also found by Suzuki and Hase for conventional SiC powders (8.7 ± 1.3 eV [25]). Reducing the HIP time to 1 h results in a density of 95% theoretical at 1430 °C. This reduction of density of about 1.7% TD/h is close to the reduction found in Fig. 7b. Also the pressure dependence, which is roughly calculated from the results at 0 and 350 MPa HIP pressure (0.043% TD/MPa), is close to our experimental results (Fig. 7a). On the other hand, the results of the model at 1500 °C without HIP pressure (about 95% TD) are significantly higher than our results for pressureless sintering (see Fig. 3). The reason is the modified pore-size distribution which is established during HIPing in an early stage. As discussed above, HIPing even at 1100 °C leads to an improved pore-size distribution (i.e. reduced mean pore diameter and pore volume) (see Fig. 5) and densities above 50% TD (see Table III). Therefore, we assume that also during the initial stage of HIPing at higher temperatures an improved pore size distribution is formed which can be described by the geometrical assumptions made in the model of Arzt *et al.* [39] (e.g. green densities of 64% theoretical or number of contacts more than 7). This is not true for the pressureless sintering, therefore the densities are significantly lower than predicted in the model.

With the modified activation energy, the model is also able to predict the densification of conventional SiC powder with a particle size of about 500 nm. Similar densities are found at temperatures which are about 250 °C higher than the temperatures needed to densify ultrafine SiC powders (see Fig. 14). This corresponds with our experimental results (Fig. 6). The model is, in principle, able to predict optimized HIPing conditions for ultrafine SiC powders. With the given parameters ($U_{gb} = 8$ eV) it gives equal densities (95% TD) for 20 min at 1542 °C and 3 h at 1400 °C. In the first case, the final grain size would be 30 nm, while for the long term HIPing a grain size of 37 nm results. This would suggest that short-term HIPing is a good method to conserve a fine grain structure. It also indicates the reason for the large grain sizes in our short-term HIP runs: the used temperatures were too high (Fig. 12); lower temperatures will be used in future experiments.

For high temperatures, the model predicts densities of 100% theoretical, which are not observed in our short-term experiments. This discrepancy can be explained by structural changes in the specimens (increasing amount of α phase with increasing temperature, see Fig. 9), which are not incorporated into the model. These changes can affect the densification by a change in the diffusion coefficients or by a change of the particle morphology leading to acicular grains; an extreme example of this process is shown in Fig. 4b.

3.4. Mechanical properties

A short summary of some thermomechanical properties will be given. In Fig. 15 the results of hardness measurements for different SiC samples are shown. A significant increase of hardness with decreasing grain size was found. This indicates a potential of nanophase SiC for tribological application. Investigations in this field are under progress. We did not find

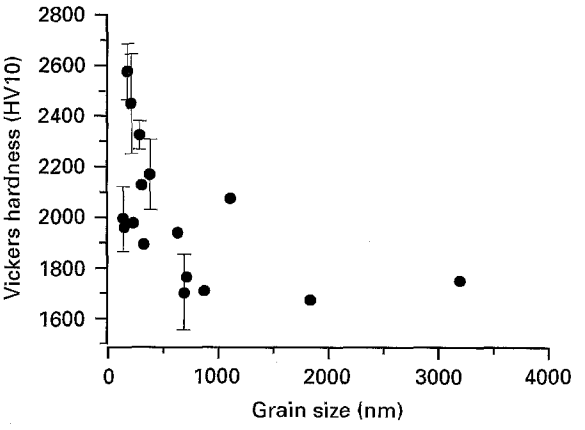

Figure 15 Effect of grain size of different SiC samples on hardness.

TABLE IX Thermomechanical properties of fine-grained SiC samples

Property	Grain size (nm)	Value
Three-point-bending strength	300	580 MPa
Thermal conductivity	180	41.5 $W m^{-1} K^{-1}$
Deformation rate at 1400 °C and > 250 MPa	130	$< 10^{-6} s^{-1}$
Hardness	200	2580
	300	2450
	390	2170
Fracture toughness	200	3.4 MPa $m^{1/2}$
	300	2.9 MPa $m^{1/2}$
	390	4.2 MPa $m^{1/2}$

a significant increase of fracture toughness with decreasing grain size. On the contrary, the values in Table IX suggest the opposite tendency. It must be borne in mind that conventional values of fracture toughness of SiC are about 4 MPa $m^{1/2}$. A similar decrease was found by Kodama and Miyoshi [29].

Hardness measurements at elevated temperatures were performed on a specimen with a grain size of approximately 370 nm. Hardness was reduced to 80.5%, 67.5% and 59.5% of the room-temperature values at 800, 1000, and 1100 °C, respectively. Fracture toughness values estimated from crack lengths indicated no increase at these temperatures. This corresponds to the low deformation rates in compression tests given in Table IX. No significant plastic deformation occurs below 1400 °C within the time scale used in indentation experiments (1 ms).

A low thermal conductivity value has been measured in the fine-grained SiC which is about half the value of conventional SiC (90 $W m^{-1} K^{-1}$ for commercially HIPed SiC). This is probably due to an increased phonon scattering at the grain boundaries.

The bending strength of 580 MPa is relatively high. This value is increased compared to conventional four-point bending test results by the relatively rather small tested volume. Nevertheless, it indicates a potential of this ceramic material.

4. Conclusion

Laser-synthesized powders with particle sizes below 20 nm have been densified by pressureless sintering and by hot isostatic pressing. Pressureless sintering was always accompanied by significant coarsening.

HIPing led to samples with full density at about 1500 °C. This is 200 °C below the temperature needed to densify conventional powders. Porosity measurements indicate that HIPing is able to improve the relatively open pore structure found after cold isostatic pressing during an early stage. HIPing of samples without boron and carbon as sintering additives led to low grain sizes and lower densities. On the other hand, the ratio of density to grain size was only slightly improved for samples without additives.

Modelling of the HIP process was performed by including grain-growth kinetics. Experimental results on grain growth could be best explained by using a $t^{1/4}$ law with an activation energy of 6.8 eV.

Consistent results on density could be achieved by increasing the activation energy for grain-boundary diffusion from 6.2 eV to 8 eV. With this parameter, the model was able to give hints for an optimized HIP schedule and gave also consistent results for the densification of conventional powders.

Nevertheless, the manufacture of fine-grained SiC ceramics remains difficult, owing to the unfavourable ratio of grain growth and densification in this material. On the other hand, interesting thermo-mechanical properties reveal the potential of this type of ceramic. This should provide stimulus for further activities in this field.

5. Acknowledgements

The authors thank Mrs Schwartz, of our Institute, for the preparation of samples and Mr Coenen and Mr Gelissen, also of our Institute, for performing the HIP experiments. The contribution of different members of the Forschungszentrum Jülich GmbH, who contributed to this work, is gratefully acknowledged. In particular, the following people are especially thanked; W. Kesternich, Institut für Festkörperforschung, for TEM sample preparation and analysis; Dr Heckner and Mr Mischulitz, Zentralabteilung für Chemische Analysen, for performing the chemical analysis; Mr Lersch, of our Institute, for performing the XRD measurements; Mr D'Orsaneo and his colleagues, Zentralabteilung Technologie, for the skilful preparation and sealing of the glass capsules. The good cooperation with the Institut für Laser- und Plasmaphysik, University Düsseldorf, and the head of the Institute, Professor Uhlenbusch, is acknowledged.

References

1. K. A. SCHWETZ, W. GRELLNER, K. HUNOLD, A. LIPP and M. LANGER, in "Ceramic Materials and Components for Engines", Proceedings of the Second International Symposium, Lübeck-Travemünde, Germany, 14-17 April 1986, edited by W. Bunk and H. Hausner (Deutsche Keramische Gesellschaft e.V., Bad Honnef, FRG, 1986), pp. 1050–62.
2. W. DIENST, T. FETT, R. HEIDINGER, H.D. RÖHRIG and B. SCHULZ, *J. Nucl. Mater.* **174** (1990) 102.
3. R. MORRELL, "*Handbook of Properties of Technical & Engineering Ceramics*", Part I (HMSO, London, 1989).
4. U. HERR, R. BIRRINGER and H. GLEITER, *Ceram. Forum Int.* **67** (1990) 70.
5. R. W. SIEGEL and J. A. EASTMAN, *Mater. Res. Symp. Proc.* **132** (1989) 3.
6. H. HAHN and R. S. AVERBACK, *Nanostruct. Mater.* **1** (1992) 95.
7. J. FÖRSTER, R. VAßEN and D. STÖVER, *J. Mater. Sci. Lett.* **14** (1995) 214.
8. M. M. R. BOUTZ, G. S. A. M. THEUNISSEN, A. J. A. WINNUBST and A. J. BURGGRAAF, *Mater. Res. Symp. Proc.* **196** (1990) 87.
9. M. J. MAYO, D.C. HAGUE and D.-J. CHEN, *Mater. Sci. Eng.* **A166** (1993) 145.
10. H.-J. MÖLLER, *J. Am. Ceram. Soc.* **68** (1985) 320.
11. C. GRESKOVICH and J. H. ROSOLOWSKI, *ibid.* **59** (1976) 336.
12. W. SYMONS and S. C. DANFORTH, in "Ceramic Materials and Components for Engines", edited by V. J. Tennery (American Ceramic Society, Westerville, OH, 1989) p. 67.

13. M. W. BARSOUM and P. D. OWNBY, *Mater. Sci. Res.* **14** (1980) 457.
14. J. FÖRSTER, M. V. HOESSLIN, J. H. SCHÄFER, J. UHLENBUSCH and W. VIÖL, in "Proceedings of the 10th International Symposium on Plasma Chemistry", Vol. 1 (U. Ehlemann, H. G. Lergon and K. Wiesemann, Buchum, FRG, 1991) p. 1.
15. J. FÖRSTER, Dissertation, Heinrich-Heine-Universität Düsseldorf (1995).
16. J. M. SCHULTZ, "Diffraction for Materials Scientists" (Prentice-Hall, Englewood Cliffs, NJ, 1982) p. 226.
17. R. VAßEN and D. STÖVER, *Powder Technol.* **72** (1992) 223.
18. M. I. MENDELSON, *Am. Ceram. Soc.* **52** (1969) 443.
19. A. G. EVANS, "*Fracture Mechanics Applied to Brittle Materials*", ASTM STP 678 (American Society for Testing and Materials, Philadelphia, PA, 1979) p. 112.
20. E. EL.-MAGD, "*Temperaturabhängigkeit dynamisch ermittelter Härte von metallischen Werkstoffen*", VDI Berichte Nr. 804 (1990) p. 411.
21. R. VAßEN and D. STÖVER, *J. Mater. Sci.* **29** (1994) 3791.
22. R. VAßEN, D. STÖVER and H.-P. BUCHKREMER, "Advances in Powder Metallurgy and Particulate Materials 1992", Vol. 7, edited by J. M. Capus and R. M. German, Proceedings of the 1992 Powder Metallurgy World Congress, 21–26 June, 1992, San Francisco, CA (Princeton, N. J., 1992) p. 19–28.
23. W. D. KINGERY and B. FRANCOIS, in "Sintering and Related Phenomena", edited by G. C. Kuczynski, N. A. Hooton and C. F. Gibson (Gordon and Breach, New York, 1967). p. 471.
24. S. PROCHAZKA, "Proceedings of the Third International Conference on Silicon Carbide", edited by R. C. Marshall, Miami Beach, Florida, 17-20 September 1973 (University of South Carolina Pr., Columbia, 1974), p. 394.
25. H. SUZUKI and T. HASE, "Proceedings of the Symposium of Factors in Densification and Sintering of Oxide and Non-oxide Ceramics", edited by S. Sumiya and S. Saito (Association of Science Documents Information, Tokyo, Japan, 1979) p. 345–365.
26. R. VASSEN, D. STÖVER and J. UHLENBUSCH, in "Euro-Ceramics II", Vol. 2, edited by G. Ziegler and H. Hausner (Deutsche keramische Gesellschaft e.V., Köln, FRG 1993) p. 791.
27. R. GILISSEN *et al*, in "Proceedings of the HIP93 Conference", 21–23 April 1993, Antwerp, Belgium, edited by J. P. Erauw, J. Schrijvers, M. Cauchtier, M. Luce and N. Herlin (Elsevier, Amsterdam) p. 354–362.
28. "Gmelin Handbook", Silicon Supplement, Vol. B2, edited by G. Kirschstein, and D. Kaschel (Springer Verlag, Berlin, 1984) p. 5.
29. H. KODAMA and T. MIYOSHI, *Adv. Ceram. Mater.* **3** (1988) 177.
30. S. SHINOZAKI and K. R. KINSMAN, in "Proceedings of the Sixth International Materials Symposium, Ceramic Microstructures 1976: with Emphasis on Energy Related Applications, edited by R. M. Fulrath, University of California, Berkeley, 24–27 August 1976, (Westview Press, Boulder, CO, 1977) p. 60–70.
31. R. BIRRINGER, U. HERR and H. GLEITER, in "Grain Boundary Structure and Related Phenomena", Proceedings of JIMIS-4 (1986), *Suppl. Trans. Jpn Inst. Metals* **27** (1986) 43.
32. A. KAISER, R. VAßEN, D. STÖVER and H. P. BUCHKREMER, *Nanostruct. Mater.* **4** (1994) 795.
33. R. J. BROOK, in "Treatise on Materials Science and Technology", Vol. 9, "Ceramic Fabrication Processes", edited by F. F. Y. Wang (Academic Press, New York, 1976) pp. 331–65.
34. I. KAUR and W. GUST, "*Handbook of Grain And Interphase Boundary Diffusion Data*", Vol. 2 (Ziegler Press, Stuttgart, 1989) pp. 1264–74.
35. J. D. HONG, M. H. HON and R. F. DAVIS, *Mater. Sci. Monogr.* **6** (1980) 409.
36. M. H. HON, R. F. DAVIS and D. E. NEWBURY, *J. Mater. Sci.* **15** (1980) 2073.
37. M. H. HON and R. F. DAVIS, *J. Am. Ceram. Soc.* **63** (1980) 546.
38. Idem, *J. Mater. Sci.* **14** (1979) 2411.
39. E. ARZT, M. F. ASHBY and K. E. EASTERLING, *Metall. Trans* **14A** (1983) 211.
40. J. J. WLASSICH and R. B. CLOUGH, in "Proceedings of the Second International Conference on Hot Isostatic Pressing: Theory and Applications", Gaithersburg, MD, 7–9 June 1989, edited by R. J. Schaefer and M. Linzer (ASM International, Materials Park, OH, 1991) pp. 123–8.
41. J. BOIKO, private communications, January 1995.
42. O. CROIX, M. GOUNOT, P. BERGEZ, M. LUCE and M. CAUCHTIER, in "Ceramics Today-Tomorrow's Ceramics", edited by P. Vincenzini (Elsevier Science, Amsterdam, 1991) pp. 1447–55.
43. K. KIJIMA, H. NOGUCHI and M. KONISHI, *J. Mater. Sci.* **24** (1989) 2924.
44. R. VAßEN, D. STÖVER and H. P. BUCHKREMER, *HIPing of Conventional Si_3N_4 and Ultrafine SiC Powder Mixtures*,in "Proceedings of the Hot Isostatic Pressing '93 Conference, Antwerp, Belgium, 1993, (Elsevier, Amsterdam, 1993) p. 363–371.
45. C. A. NANNETTI, E. BORSELLA, R. FANTONI, S. PICCIRILLO, in "Proceedings of the 7th CIMTEC-World Ceramics Congress and Satellite Symposia", Montecatini, 24–30 June 1990, edited by P. Vincenzini (Elsevier, Amsterdam, 1991) p. 1139–1148.
46. H. R. BAUMGARTNER, in "Proceedings of the 1987 SiC-Symposium", 2–5 August, edited by J. D. Cawley (American Ceramic Society, Westerville, OH, 1989) p. 3–15.
47. C. WEHLING, Dissertation, TU Berlin (1993).
48. B. BISHOP, M. S. SPOTZ, W. E. RHINE, H. K. BOWEN and J. R. FOX, *Ceram. Trans.* **1** (1988) 856.
49. M. OHKOHCHI and Y. ANDO, *J. Ceram. Soc. Jpn, Int. Edn*, **98** (1990) 4.

Received 20 September 1995
and accepted 15 January 1996